High-speed ILIDS measurement of evaporating droplet

T. Kawaguchi*, I. Satoh. and T. Saito
Dept. of mechanical and control engineering, Tokyo institute of technology, Japan
kawat@mep.titech.ac.jp

Abstract

In order to investigate the dynamic interaction between liquid and gas phases in such multiphase flows as spray and bubbly flows, the size and momentum of individual particle are the significant quantities. Moreover the improvement of multi-dimensional and spatio-temporal spray measurement technique leads us to investigate the detailed heat and mass transport phenomena, and to construct the practical computation models for numerical simulations. Interferometric laser imaging for droplet sizing (ILIDS) technique was firstly developed for the investigation of the instantaneous spatial distribution of droplet size by means of laser light source and film imaging methodology. Sizing equation was derived by considering the optical pass difference of the scattered lights from a droplet by the geometric optical approximation. Although the difficulty in discriminating the overlapped parallel fringes in the captured image was overcome by optical squeezing technique, temporal resolution was still low due to the limitation of the imaging facility. In the last decade, the drastic development of optical matrix sensor such as CCD or CMOS camera enables the dynamic measurement of flow field whose sampling frequency is over several kHz with simultaneous exposure of each pixel. Another contribution is due to the light source. Nd:YLF laser could emit the coherent light with high repetition frequency. In the present study, the single-cavity double-pulsed laser system was employed in conjunction with the synchronized high-speed camera. The relation between droplet size and fringe frequency was numerically investigated to estimate the measurement error due to the non-linear relation between them. Moreover the effect of laser sheet thickness, and of refractive index fluctuation were analyzed. The size transition of the droplets within a few milliseconds was experimentally investigated. The results led us to evaluate the mass transfer rate at the gas-liquid interface of the individual droplet.

Introduction

Such physical properties as droplet size and velocity vector and their spatial distribution are the significant parameters to characterize the spray systems. Moreover the improvement of multi-dimensional and spatial-temporal spray measurement technique leads us to investigate the detailed heat and mass transport phenomena, and to construct the practical computation models for numerical simulations. Interferometric laser imaging for droplet sizing (ILIDS) technique[1] [2] was developed for the investigation of the spatial distribution of droplet size. The ILIDS technique is the method that observes the interference between reflective and refractive rays on the out-of-focus plane. The principle of the ILIDS technique was based on Mie scattering theory, sizing method was developed by considering the optical pass difference of the scattered lights from a droplet. Although the difficulty in discriminating the overlapped parallel fringes in the captured image was overcome by optical squeezing technique[3]-[7], temporal resolution was still low due to the limitation of the imaging facility. In the last decade, the drastic improvement of optical sensor matrix such as CCD or CMOS camera enables the dynamic measurement of flow field whose sampling frequency is over several kHz with instantaneous exposure of each pixel[8]. Another contribution is the light source, Nd:YLF laser could emit the TEM_{00} coherent light with high repetition frequency. Although the previous high-power laser system, which was used for the sheet illumination such as high-speed PIV or PTV, the beam quality and energy stability were insufficient for the interferometric measurement, especially for the double-cavity oscillators. In the present study, the single-cavity double-pulsed laser system was firstly employed in conjunction with the synchronized high-speed camera, and performed the Lagrangian investigation of the evaporating liquid droplet in heated air jet.

Sizing accuracy of ILIDS

One of the significant advantages of the ILIDS technique is that the diameters of particles are obtained not by the intensity information but by the spatial frequency of fringe. Consequently the well-established spectral analysis method such as burst signal processing for laser Doppler velocimetry could be applied to the size determination. In the image analysis of ILIDS technique, the discrete power spectrum provides a broad distribution and presents difficulties in the determination of the fine peak frequency of fringe, especially at the midpoint between the channels

*Corresponding author: kawat@mep.titech.ac.jp

of fundamental frequency. Since the measured droplet size is assumed to be linearly proportional to the fringe frequency, the accuracy of frequency determination is directly connected to the sizing accuracy. Therefore the fitting method for peak determination with sub-pixel accuracy in the frequency domain is quite important for the accurate tracking of droplet size change and for the evaluation of the mass transfer rate. The interpolation technique enables to improve the resolution of finding the peak frequency of interferometric signals and to enhance the resolution of the measured diameter. The amount of the adjustment is simply calculated by using the Gaussian function fitting, which considers the peak power and neighboring power in the discrete spectrum. Denoting by k, the integer index of the peak frequency in the power spectrum, the modified frequency is described as follows.

In the simplified case, the parabolic function fitting could be applied;

$$a = \frac{1}{2}\left(\frac{P_{k-1} - P_{k+1}}{P_{k-1} - 2P_k + P_{k+1}}\right) \tag{1}$$

Gaussian function interpolation is another fitting method;

$$a = \frac{1}{2}\left(\frac{\ln P_{k-1} - \ln P_{k+1}}{\ln P_{k-1} - 2\ln P_k + \ln P_{k+1}}\right) \tag{2}$$

By using the equation (1) or (2) in conjunction with the following refinement of integer frequency, f_k, the fine peak frequency could be estimated.

$$f = f_k + a \tag{3}$$

$$f = f_k + 0.9169a + 0.3326a^3 \tag{4}$$

The conventional Gaussian fitting method by equation (2) and (3) remarkably reduces the bias error of the calculated frequency to less than 1% for the fundamental frequency. Moreover, the polynomial adjustment by equation (4) reduces the residual bias, the resultant error for absolute diameter could be reduced to less than 0.02% [9].

In the previous reports[3], such statistical error analysis as the mean diameter, phase-averaged velocity vector of the spray characteristics were studied, however, neither the error due to the simplified geometric optical approximation nor the resonance effect of the Mie scattering was investigated. The detailed sizing criteria and error analysis would be necessary to estimate the mass transfer rate of the evaporation droplets.

$$d = \frac{2\lambda N}{\alpha}\left(\cos(\theta/2) + \frac{m\sin(\theta/2)}{\sqrt{m^2 - 2m\cos(\theta/2) + 1}}\right)^{-1} \tag{5}$$

In the sizing equation (5), the scattering angle θ, collection angle α and wavelength λ were the fixed value and independent to the fluid flow. Refractive index m and fringe number N might be varied due to the fluid flows and should be considered. Moreover the equation (5) is derived by using the geometric optics, the error come from the approximation has to be estimated. In the following section, (i) the effect of the laser sheet thickness, (ii) accuracy of the g.o. approximation, (iii) refractive index effect was investigated.

Figure 1 depicts the experimental setup. The system consisted of DM10-527 (Photonics Industries International Inc.), double-pulsed Nd:YLF laser with light sheet optics and a camera with an anamorphic focusing optics and a rectangular aperture. A couple of cylinder lens were used to adjust the laser sheet thickness. The maximum output power and single pulse energy of the laser system were 14 W and 10 mJ. If the velocity magnitude of the fluids flow is very low, continuous-wave (CW) laser could be applied to the interferometric measurement. Wavelength of Nd:YLF laser is 527 nm that is almost the same as the frequency-doubled Nd:YAG laser. Since the sensitivity of the imaging sensor is maximum around 530 nm of wavelength, signal to noise ratio of the captured image becomes high. Duration of the laser pulse was 220 ns approximately, repetition frequency was 4000 Hz, consequently the temporal resolution was 0.25 ms. The MotionXtra N4 (IDT Corp.) high-speed CMOS camera with gigabit Ethernet data transfer interface was employed for the image acquisition, which has 1016×1016 pixels, 10 bit grayscale accuracy. The maximum frame rate is 3000 fps under full-resolution. In this experiments, pixel number and frame rate were set to 512×512 pixels and 4000 fps. Both image acquisition system and pulsed laser system were synchronized with the low voltage TTL trigger signal. Internal memory capacity of the camera system was 1.3 GB, resultant duration of the overall image acquisition, which depends on the frame rate of the camera, was several hundred milliseconds to 1 ms approximately. Scattering angle and collection angle was set to θ=65 degree and α=10 degree respectively. The focal point of the receiving optics was located behind the laser

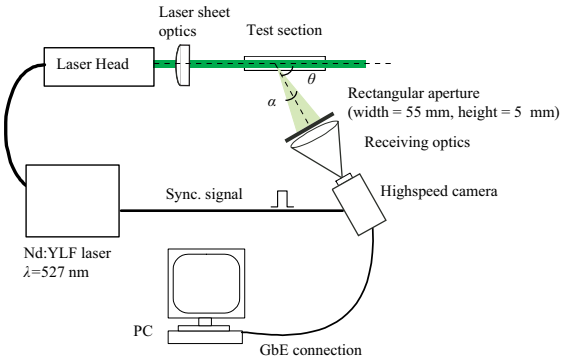

Figure 1. Experimental set-up of the interferometric laser imaging system. The measurement system consisted of a high-speed camera, defocusing optics with a rectangular aperture, Nd:YLF laser with a laser sheet optics and personal computer for the image processing. Both camera and laser equipment were synchronized by the electric signal.

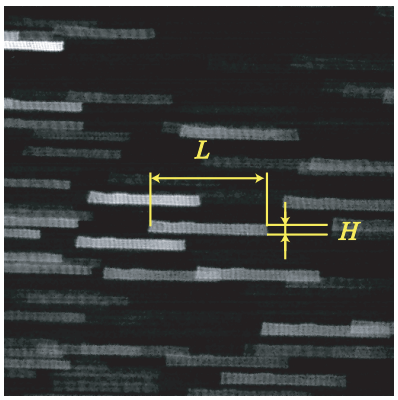

Figure 2. An example of the captured image. Each rectangular interferogram corresponds to a droplet, the frequency of the fringe is proportional to the diameter of droplet. The rectangular shape of the interferogram is due to the shape of the aperture in front of the receiving lens in Figure 1. Physical dimension of the image is 14 mm $\times$ 14 mm.

sheet. The rectangular aperture was used. The size of the aperture was 55 mm$\times$5 mm. The volume of the test section was determined by the magnification ratio of the receiving optics and the size of the CMOS sensor as well as the laser sheet thickness. The size of the volume was $14\ \mathrm{mm} \times 14\ \mathrm{mm} \times 5\ \mathrm{mm}$.

Figure 2 is an example of the captured image in the present measurement system. The shapes of the individual rectangular fringe are due to the rectangular aperture. The size of the rectangle in the image was $L = 150$ pixel and $H = 15$ pixel. Image sequence was firstly stored into the internal memory of the camera, and transferred into the computer via GbE connection. The images were processed by the image processing software to determine the particle size and velocity vectors. Such optical facilities of ILIDS as pulsed laser with light sheet optics, digital camera and image processing software are identical as conventional PIV technique. Although the fundamental studies of the multi-dimensional simultaneous size and velocity measurement of individual droplet in denser spray has been performed by Maeda *et al.*[3], the temporal resolution of the measurement was only 15 Hz due to the limitation of the frame rate of CCD camera and repetition rate of Q-switched Nd:YAG laser as well. In contrast to the previous ILIDS works, fringe image was captured in every 0.25 ms in the present experiments.

Effect of the laser sheet thickness

When the flow field is assumed to be two-dimensional or the out-of-plane component of the velocity vector is negligible, the thin laser sheet could be applicable. However, the particle behavior in turbulence such as spray flow is fully three dimensional due to the complicated interaction between dispersed and continuous phases. Under the previous ILIDS technique, the laser sheet thickness must be small for the higher intensity of illumination. The representative thickness was 100 μm to 500 μm for droplet sizing, 1 mm for the bubble sizing.[4]. In the previous ILIDS that employ the double-pulsed Nd:YAG laser, a couple of images are sufficient for the velocity measurement. Since the time interval between two image acquisition was 1 μs to several ten μs, the rejection rate of the fringe pairing was only few % in terms of the particle velocity and the pixel size in physical domain of the imaging system. Moreover the displacement of the interferogram was estimated by the cross correlation method assuming that the droplet size is identical between two images. For example, the out of plane velocity is 10 m/s and laser pulse interval is 5 μs, the resultant displacement is only 50 μm. The value is sufficiently smaller than the laser sheet thickness.

In order to estimate the mass transfer rate of the evaporating droplet, the temporal droplet size transition must be measured and the droplet trajectories were captured during several image frames. The required temporal duration of the droplet tracking is a few ms depending on the evaporation rate. Therefore the thicker laser sheet has to be used in order not to lose the droplet images.

In the actual sizing procedure, the fringe number N was estimated not only by the spatial frequency of the fringe image but also the fringe image width. Figure 3 compares fringe image variation in terms of the horizontal position in the image. Each plot corresponds a droplet, laser sheet thickness was 0.5 mm and 2.0 mm. By the thick

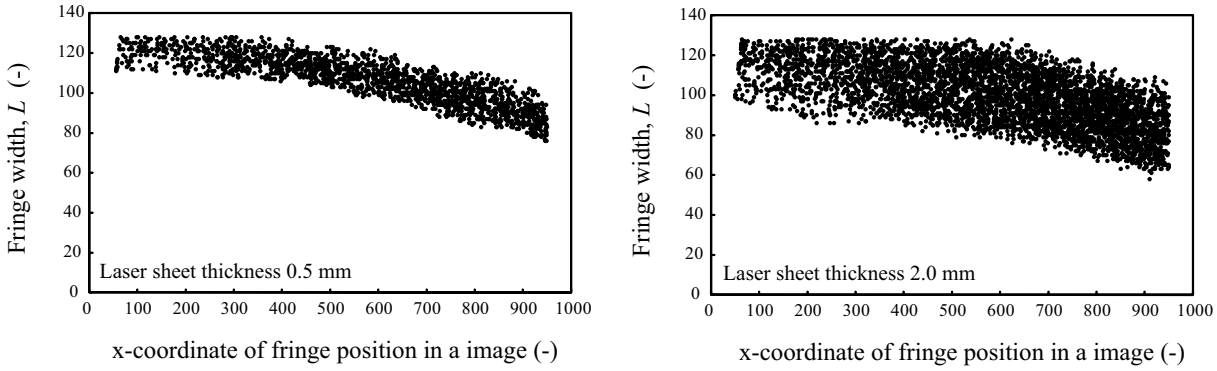

Figure 3. Measured fringe image length as a function of the x coordinate in the image, and the dependency on the laser sheet thickness. Thick laser sheet disperses the fringe image length. As increase the x coordinate, mean value of fringe width is decreased due to the off-axis alignment of the receiving optics.

laser sheet illumination, the variation of the fringe width was increased whereas the mean value of the fringe width is identical. If the thickness is very small, no variance of the particle location within the laser sheet is observed. Since the laser sheet thickness was relatively larger in the present study, the image size of individual droplet, L and H, have to be determined by image processing.

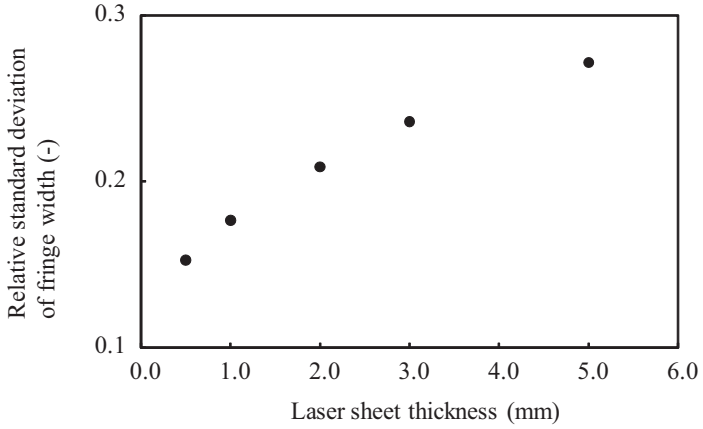

Figure 4. Relative variation of the measured fringe width in terms of the laser sheet thickness.

Figure 4 summarize the relation between laser sheet thickness and variance of the fringe image length. The standard deviation of the image length was divided by the mean value. The thickness was varied from 0.5 mm to 5 mm. The result shows that the variance of the fringe image width is increased by increasing the thickness of the laser sheet.

Approximation error of sizing equation

In the section, the error due to the geometric optical approximation was investigated by exact Mie result. Figure 5 is the computed relation between diameter and fringe number. Three different fitting function, parabolic, Gaussian and adjusted Gaussian fitting were compared. Each plot was calculated by the power spectrum analysis of the angular intensity distribution obtained by Mie scattering computation. Diameter range is from 20 μm to 40 μm, refractive index is 1.36 due to our experimental configuration. The number of DFT points was 1024, angular resolution of Mie computation is 0.01 degree, collection and scattering angle were 10.24 degree and 65 degree respectively. The solid line in the figure is the conversion relation by the sizing equation derived from geometric optical approximation. By the numerical comparison of the fitting functions, the adjusted Gaussian fitting method gives the best approximation of the droplet sizing. By comparing the approximated relation and Mie computation results, the mean value of the conversion error was less than 1% for the larger droplet, therefore the effect of the nonlinear relation to the estimation of the mean diameter as well as the variance is not remarkable.

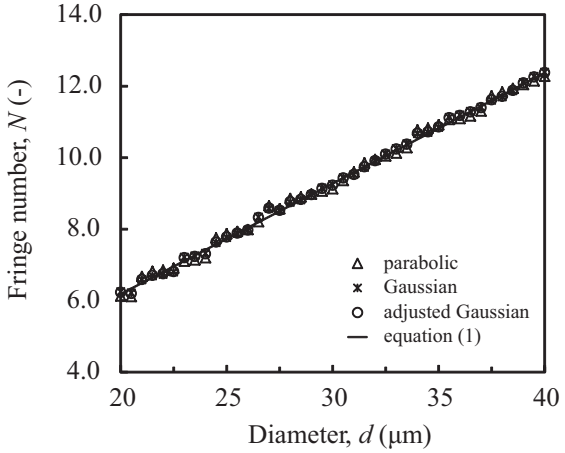

Figure 5. Relation between droplet diameter and fringe number. The plots compare the dependency on the spectral fitting functions for the analytical Mie solution. Solid line is given by the sizing relation of equation (5).

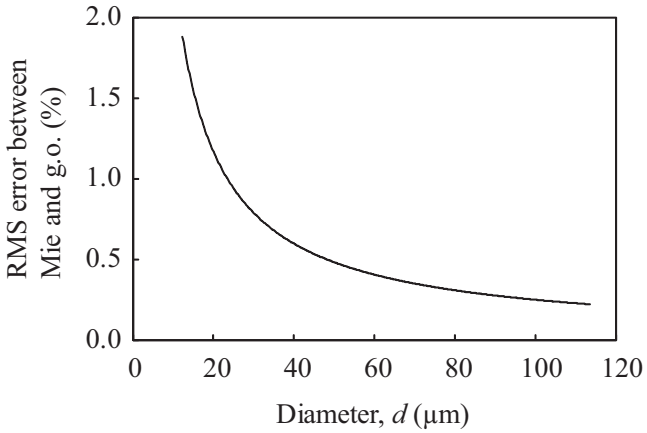

Figure 6. Sizing error due to the geometric optical approximation in terms of the diameter.

Figure 6 summarize the relative value of RMS error between Mie solution and geometric optical approximation as a function of the droplet diameter. The result shows that the absolute error was independent to the size, the relative error, however, increased for the smaller droplet.

Refractive index effect

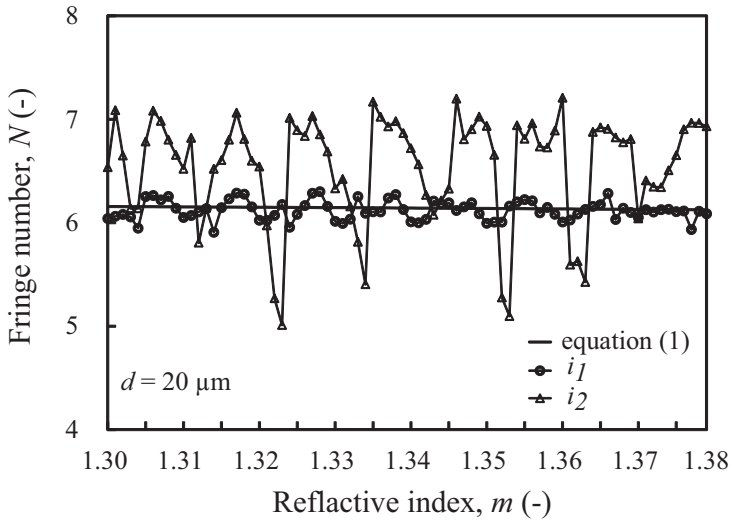

Figure 7. Fringe count dependency on the refractive index in terms of the polarization of light. i_1 and i_2 represent the perpendicular and parallel polarization lights, respectively. Diameter and wavelength are 20 μm and 527 nm. Scattering angles is 65 degree, collecting angle is 10.24 degree.

In the high temperature environment, internal temperature of the droplet was fluctuated as a consequence of the heat transfer between phases. In our previous works, refractive index is assumed to be constant under isothermal flow field[6], or could be ignored even in the vicinity of the heated surface[10]. In general, the magnitude of the refractive index fluctuation due to the temperature change is not significant. For example, refractive index change of water is 0.2% between 273.15 K and 373.15 K. The temperature effect of the refractive index modulation is 0.02% for water, 0.1% for ethanol droplet.

Figure 7 shows the fringe number modulation as a function of the refractive index of droplet. The diameter was

20 μm, the range of the refractive index was from 1.30 to 1.38. Angular intensity resolution of Mie computation was 0.01 degree. Two different linearly polarized light, i_1 and i_2, was compared. Scattering and collection angle was set to 65 degree and 10.24 degree. The result shows that the perpendicular polarization, i_1, resulted the better uniformity of the conversion relation. In contrast, the parallel polarized light, i_2, resulted more than 20% error with several discontinuity even within the slight change of the refractive index.

Experiment and result

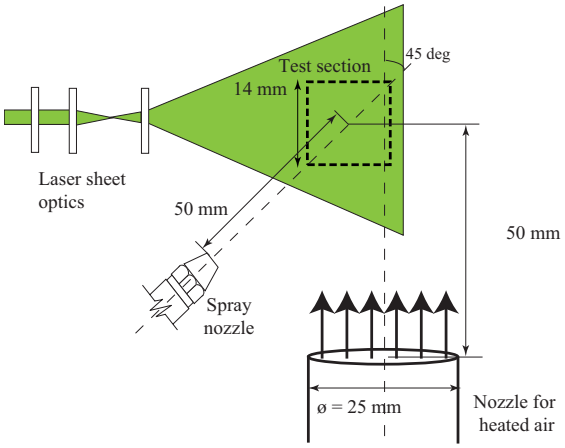

Figure 8. The alignment of the spray nozzle, round nozzle for the heated air and laser sheet. The size and location of the test section are depicted.

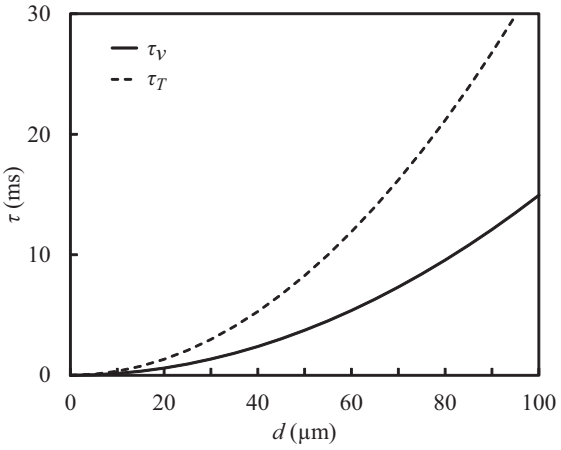

Figure 9. Relaxation times of momentum and temperature of ethanol droplet in terms of a diameter. Solid and dashed lines represent the relaxation times of momentum and temperature respectively.

Figure 8 illustrates the experimental setup for the measurement of the evaporating droplet in a heated air. The rig consisted of a round jet and spray nozzle. In order to compare the response of droplet with different Stokes number, the angled spray nozzle was installed. The spray nozzle was DELAVAN solid cone nozzle, ethanol was used as a working fluid. By using the spray nozzle, both size and velocity of droplet were varied. Initial temperature of liquid ethanol was 293 K. Mean diameter and velocity magnitude of the droplet at 40 mm from the nozzle was 60 μm and 7.3 m/s respectively. For the heated air supply, a stainless axisymmetric nozzle with internal diameter of 25 mm was used that was located under the test section. The air was heated by an electric heater, the mean temperature was 570 K. Mean velocity of the heated air, which is determined by the volume flow rate and area of the cross section of the nozzle, was $u_c = 20.0$ m/s. From the internal diameter of nozzle, $\phi = 25$ mm and kinematic viscosity of air, ν, Reynolds number of a heated air was $(u_c\phi)/\nu = 4 \times 10^4$.

Figure 9 is the relaxation time of momentum, τ_v, and that of temperature,τ_T, of ethanol droplet under the present configuration. The time constants were calculated as the following equation.

$$\tau_v = \frac{\rho_d d^2}{18\mu_c} \qquad \tau_T = \frac{\rho_d c_d d^2}{12 k_c} \tag{6}$$

Density and specific heat of ethanol were $\rho_d = 785$ kg/m^3 and $c_d = 2422$ J/kg $\cdot$ K. Viscosity and thermal conductivity of air were $\mu_c = 2.92 \times 10^{-5}$Pa $\cdot$ s and $k_c = 4.8 \times 10^{-2}$ W/m $\cdot$ K respectively. From the calculated result shown in Figure 9, the relaxation times of $d = 50$ μm droplet were τ_v=3.7 ms and τ_T=8.3 ms. The time constants were much longer than the sampling interval by the measurement system.

From the measured results, the trajectories of droplet whose signal to noise ratio of interferogram is over 10 dB was depicted in figure 10. The actual size of the measurement area was 14 mm×14 mm. The plot in the figure corresponds to the droplet location, the arrows from each plot represents the velocity vector. The initial diameter of the droplets was appeared in the vicinity of the first position on the image The axis of the heated air jet was located at $x = 12.5$ mm. From the velocity distribution, the velocity magnitude of the droplet around the axis of the heated air was faster than that of the out-of-axis area.

Figure 11 compare the temporal transition of the square of droplet diameter. The droplet A and B that are indicated in figure 10 are compared. Both droplets has similar diameter but different surrounding environment

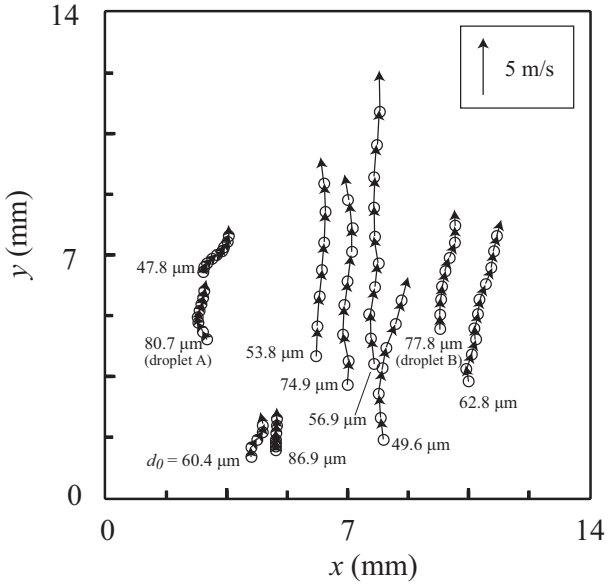

Figure 10. Measured particle trajectories by particle tracking. Hollow circles and corresponding arrows represent the instantaneous droplet locations and the individual velocity vector respectively. Frame rate of the image acquisition is 4000 Hz, consequently the temporal resolution of the droplet sizing and velocimetry is 0.25 ms. Initial droplet diameters are depicted in the vicinity of the initial droplet locations.

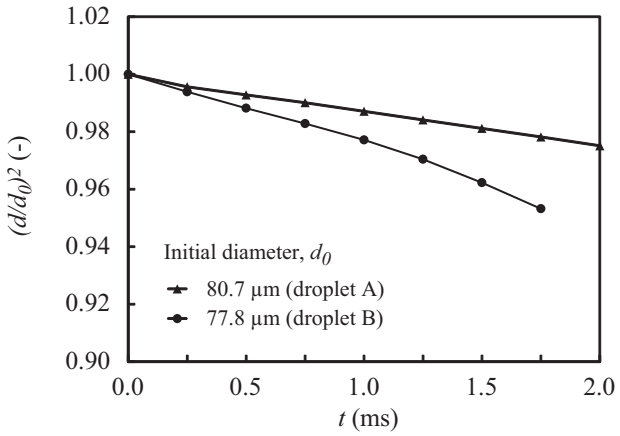

Figure 11. Temporal size transition of droplets. Initial diameters are almost the same, however, the particle location is different. The droplet B is located in the vicinity of the axis of a heated jet, and has relatively higher rate of the size reduction.

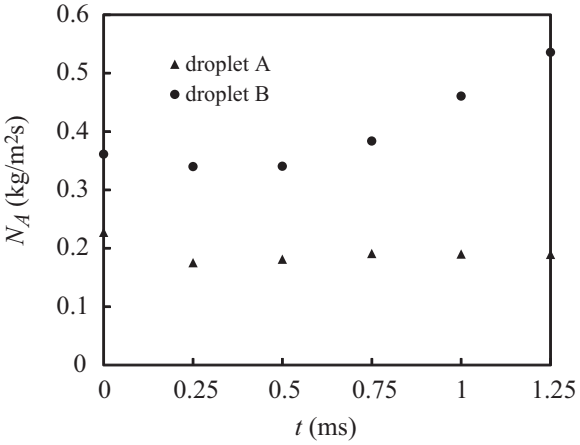

Figure 12. Comparison of mass transfer rate between two droplets located in the different environment.

such as relative velocity. The initial location of the droplet A was $x = 3.0$ mm, $y = 4.3$ mm in figure 10, that of droplet B was in the vicinity of the axis of the heated air at $x = 9.6$ mm, $y = 4.5$ mm.

Assuming that the droplet is sphere, mass flux at the gas-liquid interface was defined as follows.

$$N_A = \rho_d \frac{dV}{dt}/A = \rho_d \frac{dV}{dr}\frac{dr}{dt}/A = \rho_d \frac{dr}{dt} \tag{7}$$

A and V are the surface area and volume of droplet respectively. r is equivalent to $d/2$, ρ_d is a density of liquid. Figure 12 is the calculated mass flux by the size transition and equation (7). By the estimated result, N_A of droplet A was 0.18 $\mathrm{kg/m^2 \cdot s}$ and almost constant during the measurement duration. In contrast, N_A of droplet B was 1.6 times as large as that of droplet A, moreover the value was increased to 0.52 $\mathrm{kg/m^2 \cdot s}$ within 1 ms.

From the figure 9, thermal relaxation time of both droplets was 20 ms, the droplet was not sufficiently heated by the air. Mean value of N_A at the left-half area of the test section was $0.20\ \mathrm{kg/m^2 \cdot s}$, that of the right-half area was $0.61\ \mathrm{kg/m^2 \cdot s}$. The higher mass transfer rate was observed in the vicinity of the axis of the heated air.

By the d^2 raw[11, 12], mean value of the evaporation rate constant of droplet A and B was $K = 7.87 \times 10^{-8}\ \mathrm{m^2/s}$, $K = 15.7 \times 10^{-8}\ \mathrm{m^2/s}$ respectively. The result shows that the droplets surrounded by the different environment have different evaporation behavior even with the same initial diameters. Assuming that the evaporation rates are constant, the estimated evaporation time, $\tau_d = d_0^2/K$ of the aforementioned droplet A and B were 82.6 ms and 38.6 ms respectively.

Conclusion

The instantaneous size and velocity fields of evaporating ethanol droplet in a heating jet were measured consecutively at a high frame rate imaging system. A preliminary estimation of the sizing error was numerically investigated by Mie solution and function fitting technique. The accurate diameter determination by the spectral interpolation technique enables to find the corresponding particles between the image pair for the Lagrangian particle tracking. The technique was applied to the investigation of the evaporating ethanol droplets with a heated air jet and evaluated the evaporation rate of individual droplet.

References

[1] Hesselbacher, K.H., *et al.* "Experimental investigation of Gaussian beam effects on the accuracy of a droplet sizing method" *Appl. Opt.*, Vol. 30, pp. 4930–4935. (1991)

[2] Glover, A. R., *et al.* "Interferometric laser imaging for droplet sizing: a method for droplet-size measurement in sparse spray systems", *Appl. Opt.*, Vol. 34 pp. 8409–84–21, (1995)

[3] Maeda, M., *et al.* "Novel Interferometric Measurement of Size and Velocity Distributions of Spherical Particles in Fluid Flows", *Meas. Sci. Technol.*, Vol. 11, pp. L13–L18, (2000)

[4] Kawaguchi, T., *et al.* "Size measurements of droplets and bubbles by advanced interferometric laser imaging technique", *Meas. Sci. Technol*, Vol. 13, pp. 308–316, (2002)

[5] Kobayashi, T., *et al.* "Measurement of spray flow by an improved interferometric laser imaging droplet sizing (ILIDS) system", *Laser Techniques for Fluid Mechanics. (Springer)*, pp. 209–220, (2002)

[6] Maeda, M., *et al.* " Improvements of the interferometric technique for simultaneous measurement of droplet size and velocity vector field and its application to a transient spray", *Exp. in Fid.*, Vol. 33, pp. 125–134, (2002)

[7] Kawaguchi,T. and Maeda, M. "Measurement technique for analysis in two-phase flows involving distributed size of droplets and bubbles using interferometric method", *Multiphase Sci. and Technol.*, Vol. 17, pp. 57–77, (2005)

[8] Lee,S.J., *et al.* "Dynamic PIV Measurement of a Compressible Flow Issuing from an Airbag Inflator Nozzle", *Journal of Thermal Science*, Vol.15, No.4, 377–381, (2005)

[9] Kobashi, K., *et al.* "Measurement of fuel injector spray flow of I.C. engine by FFT based phase Doppler anemometer" *Application of Laser Techniques to Fluid Mechanics. (Berlin: Springer)*, pp. 268–287, (1990)

[10] Kawaguchi, T., *et al.* "Planar Measurement of Local Characteristics of Impinging Spray on Heating Plate" *Proceedings of the 6th ASME-JSME Thermal Engineering Joint Conference*, TED–AJ03–370, (2003)

[11] Abramzona,B. and Sirignanoa,W.A., "Droplet vaporization model for spray combustion calculations", *International Journal of Heat and Mass Transfer*, Vol.32, 9 (1989), pp.1605–1618.

[12] Sirignano,W.A., *Fluid Dynamics and Transport of Droplets and Sprays*, Cambridge University Press, Cambridge (1999).